PAPER

Structural and magnetic phase transitions in $Cs_2[FeCl_5(H_2O)]$

IOP Publishing Journal of Physics: Condensed Matter
J. Phys.: Condens. Matter **30** (2018) 295403 (10pp) https://doi.org/10.1088/1361-648X/aaca6c

Structural and magnetic phase transitions in $Cs_2[FeCl_5(H_2O)]$

Tobias Fröhlich[1], Jonas Stein[1], Ladislav Bohatý[2], Petra Becker[2], Arsen Gukasov[3] and Markus Braden[1]

[1] II. Physikalisches Institut, Universität zu Köln, Zülpicher Straße 77, 50937 Köln, Germany
[2] Abt. Kristallographie, Institut für Geologie und Mineralogie, Universität zu Köln, Zülpicher Straße 49b, 50674 Köln, Germany
[3] Laboratoire Léon Brillouin, CEA-CNRS, CEA/Saclay, 91191 Gif sur Yvette, France

E-mail: tfroehl3@uni-koeln.de

Received 21 March 2018, revised 1 June 2018
Accepted for publication 5 June 2018
Published 27 June 2018

Abstract

The compound $Cs_2[FeCl_5(H_2O)]$ is magnetoelectric but not multiferroic with an erythrosiderite-related structure. We present a comprehensive investigation of its structural and antiferromagnetic phase transitions by polarization microscopy, pyroelectric measurements, x-ray diffraction and neutron diffraction. At about (157.6 ± 0.1) K, the compound changes its symmetry from *Cmcm* to *I*2/*c*, with a doubling of the original *c*-axis. This transformation is associated with rotations of the $[FeCl_5O]$ octahedra and corresponds to an ordering of the H_2O molecules and of the related H bonds. A significant ferroelectric polarization can be excluded for this transition by precise pyrocurrent measurements. The antiferromagnetic phase transition occurring at 6.4 K results in the magnetic space group $I2'/c$, which perfectly agrees with previous measurements of the linear magnetoelectric effect and magnetization.

Keywords: erythrosiderite, polarization microscopy, pyroelectricity, x-ray diffraction, neutron diffraction, crystal structure, magnetic structure

(Some figures may appear in colour only in the online journal)

1. Introduction

In 2013 it was found that $(NH_4)_2[FeCl_5(H_2O)]$, whose crystal structure was determined in 1978 [1] and further investigated in 2013 [2], is multiferroic with a strong magnetoelectric coupling [3]. It is a member of the family of erythrosiderite-related compounds with general composition $A_2[FeX_5(H_2O)]$, wherein A is an alkali metal or an ammonium ion, and X is a halide ion. In order to investigate the magnetoelectric coupling of this multiferroicity, the composition was varied by introducing several alkali metals $A = K, Rb, Cs$ [4]. Erythrosiderite-type compounds exhibit low Néel temperatures ranging from 6 K to 23 K [5, 6] due to the large Fe–Fe distances and the correspondingly small magnetic exchange.

In contrast to $(NH_4)_2[FeCl_5(H_2O)]$, $A_2[FeCl_5(H_2O)]$ with $A = K, Rb, Cs$ are not multiferroic, but magnetoelectric [4]. Furthermore, $(NH_4)_2[FeCl_5(H_2O)]$ shows two sequent magnetic phase transitions, as observed by heat capacity measurements [7], of which the second phase transition coincides with the onset of electric polarization [3]. In contrast, the alkali-metal compounds exhibit only a single magnetic phase transition [8, 9].

At room temperature, the crystal structures of $A_2[FeCl_5(H_2O)]$ with $A = NH_4, K, Rb$ are orthorhombic with space group *Pnma*, while for $A = Cs$, the space group is *Cmcm*. In all these materials, the crystal structure consists of $[FeCl_5(H_2O)]$ octahedrons forming zig-zag chains and of A ions or molecules occupying the space between these zig-zag chains. While for the *Pnma* structures, the zig-zag chains run along the *b* axis, for $Cs_2[FeCl_5(H_2O)]$ the chains are oriented along the *c* axis. A further difference concerns sizeable disorder of the O–H–Cl bonds in the case of $Cs_2[FeCl_5(H_2O)]$.

The room temperature structure of $Cs_2[FeCl_5(H_2O)]$ contains octahedrons $[FeCl_5(H_2O)]$ with an Fe^{3+} ion in the center, four Cl atoms in the equatorial plane, and one Cl-atom and a H_2O molecule occupying the apical corners [10], see figure 1(a). The octahedrons are tetragonally distorted in the way that the O ion and the opposing Cl-atoms show a

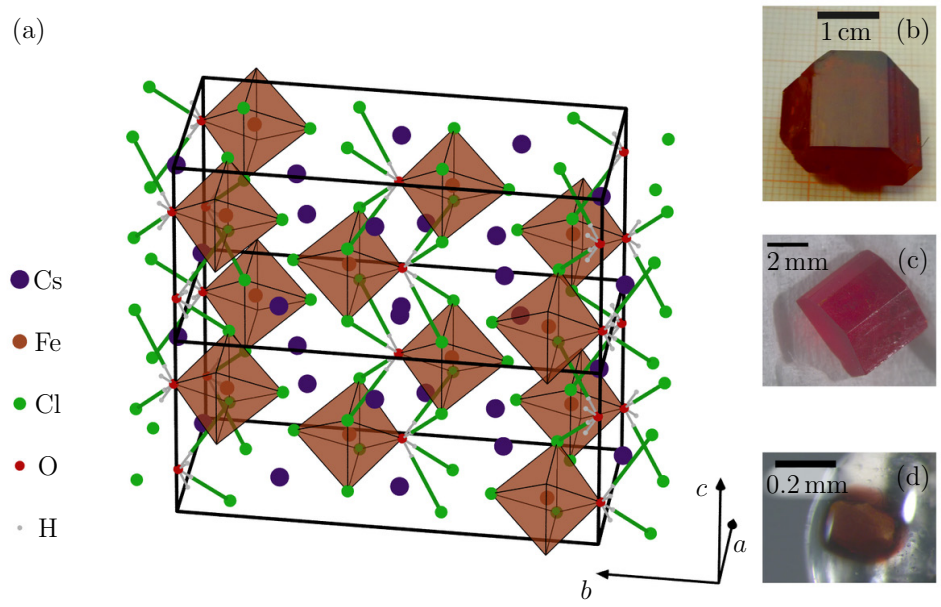

Figure 1. (a) Room temperature structure of $Cs_2[FeCl_5(H_2O)]$. The gray lines represent O–H hydrogen bonds and the green lines represent H–Cl hydrogen bonds. In the high temperature space group *Cmcm*, the bonds are disordered, so that there are two possible Cl Atoms and H positions for each bond. The structure was determined by x-ray diffraction according to table 2. For this figure, the positions of the H atoms are assumed to lie on the connecting line O–Cl with a distance from the O atom of 0.83(10) Å according to [10]. The figure shows two unit cells stacked, for easy comparison with the low temperature structure. (b) Crystal of $Cs_2[FeCl_5(H_2O)]$ with well-developed morphological faces. (c) Sample used for neutron diffraction. (d) Sample used for x-ray diffraction.

smaller distance from the Fe atom compared to the equatorial Cl atoms [8]. The octahedrons are connected via O–H–Cl hydrogen bonds forming a zig-zag line along the *c* axis. The Cs atoms occupy the space between the octahedrons. At room temperature, the hydrogen bonds are fully disordered. Around each O site there are four equivalent Cl atoms to which a hydrogen bond can be attached through a single H_2O molecule. The hydrogen atoms and the entire H_2O molecule must hop between different potential minima, while in an ordered arrangement only two hydrogen bonds would form out of these four possibilities. This is illustrated in figure 1(a), where all four equivalent bonds are drawn.

In the compounds with $A = \mathrm{K}, \mathrm{Rb}$, the magnetic easy axis is the *a* axis. This is also true for $A = \mathrm{Cs}$. However—as mentioned above—the zig-zag chains are oriented in a different way in the Cs case. All octahedron centers of a zig-zag chain approximately lie in the same plane, which is the *a*-*b* plane for $A = \mathrm{K}, \mathrm{Rb}$ and the *b*-*c* plane for $A = \mathrm{Cs}$. The magnetic easy axis lies within this plane for the former cases and is oriented perpendicular to this plane in the Cs case. The compound $(NH_4)_2[FeCl_5(H_2O)]$ does not exhibit a magnetic easy axis but an easy plane. The magnetic moments of $(\mathrm{K}/\mathrm{Rb})_2[FeCl_5(H_2O)]$ and $Cs_2[FeCl_5(H_2O)]$ span the same plane as the moments of the cycloidal structure of $(NH_4)_2[FeCl_5(H_2O)]$ with respect to the zig-zag chain. This indicates that the multiferroic cycloidal order of $(NH_4)_2[FeCl_5(H_2O)]$ is induced by Dzyaloshinskii–Moriya interaction and by the presence of an easy-plane anisotropy, which facilitates cycloidal order [4, 11].

While the crystallographic and magnetic structures as well as the magnetic properties of $K_2[FeCl_5(H_2O)]$ and $Rb_2[FeCl_5(H_2O)]$ are exhaustively investigated [7, 9, 12–14] yielding a magnetic structure with magnetic space group $Pn'm'a'$, only the magnetic structure of the deuterated Cs compound $Cs_2[FeCl_5(D_2O)]$ has recently been reported [15]. Furthermore, $Cs_2[FeCl_5(H_2O)]$ exhibits a structural phase transition at about 151.5 ± 0.5 K. This structural phase transition was discovered via Mössbauer spectroscopy in 1987 [16], but not taken into account for several decades.

Magnetization measurements on $Cs_2[FeCl_5(H_2O)]$ reveal an antiferromagnetic ordering at $T_N = 6.4$ K and suggest ordered moments pointing along *a*. $Cs_2[FeCl_5(H_2O)]$ furthermore exhibits a spin-flop transition at a magnetic field of $B_{\mathrm{SF}} \approx 1.2$ T along the *a* direction, wherein the spins rotate from being aligned parallel to the *a* axis to lying within the plane perpendicular to the *a* axis [4]. The Weiss temperature has been determined to be $\theta = -12$ K [4], which is a further indication for an antiferromagnetic coupling. The frustration parameter [17] can be calculated to be $f = \theta/T_{\mathrm{c}} = 1.9$ indicating only moderate frustration.

By investigating the magnetoelectric effect and the magnetization and assuming a $\boldsymbol{q} = \boldsymbol{0}$ magnetic structure, it was possible to predict the antiferromagnetic space group to be [4]:

$$C\frac{2}{m}\frac{2}{c}\frac{2_1}{m} \mapsto C\frac{2'}{m}\frac{2'}{c}\frac{2_1}{m'}. \tag{1}$$

In the present study, the crystallographic phase transition occurring at ∼160 K has been investigated via polarization microscopy, x-ray-diffraction and pyroelectric measurements and the antiferromagnetic phase transition at 6.4 K by means of neutron diffraction yielding perfect agreement with the

macroscopic and microscopic studies in [4, 18, 19]. This paper is structured as follows: First, the crystal growth and experimental setups are described. Then the results are presented and analyzed with respect to its symmetric and structural properties. In the conclusion, we compare the magnetic and crystal structure of $Cs_2[FeCl_5(H_2O)]$ with that in related erythrosiderites.

2. Experiments

Single crystals of $Cs_2[FeCl_5(H_2O)]$ were grown from aqueous solution of CsCl and $FeCl_3$ in a ratio of 2 : 1 with surplus of hydrochloric acid. Growth by controlled slow evaporation of the solvent at different (constant) temperatures as well as growth driven by temperature decrease was performed. Best results in our growth experiments were obtained by controlled slow evaporation of the solvent at constant temperature of 323 K. Within growth periods of 10–12 weeks, optically clear red crystals of dimensions up to $15 \times 20 \times 25\,\mathrm{mm}^3$ with well-developed morphological faces were grown, see figure 1(b). The morphological faces (see [4]) were used as reference faces for the orientation of the crystals during sample preparation.

For temperature-dependent polarization microscopy, plate-shaped samples of orientations $(1\,0\,0)$, $(0\,1\,0)$ and $(0\,0\,1)$ with thicknesses between 0.18 mm and 0.34 mm and with polished faces were prepared. The samples were investigated in the temperature range 100 K–300 K using a polarization microscope equipped with a Linkam cooling stage with LN_2 cooling.

Pyroelectric measurements were performed using a home-made setup for the measurement of the pyroelectric charge (Keithley 6517b electrometer) and a plate-shaped sample of 0.88 mm thickness and a plate area of $4.4 \times 4.0\ \mathrm{mm}^2$. Pyroelectric measurements were carried out during sample heating cycles after cooling the sample in an applied static electric field with a temperature rate of about 3–5 K min^{-1}. The field was applied with two different signs with field strengths of 0.568 kV mm^{-1} or 1.705 kV mm^{-1}.

For neutron diffraction experiments, a large single crystal sample with dimensions of roughly $5 \times 5 \times 2$ mm was prepared, see figure 1(c). Neutron diffraction experiments were carried out at the thermal neutron four-circle diffractometer 6T2 with lifting counter at the Laboratoire Léon Brillouin (Saclay, France). The sample was mounted with the b axis vertical to the scattering plane in a ^{4}He cryostat and a wavelength of 0.9 Å was chosen. One magnetic and one nuclear superstructure reflection were measured as function of temperature, and sets of Bragg reflection intensities were recorded at 1.6 K below the Néel temperature and at 10 K above.

By x-ray diffraction, the splitting of a Bragg reflection was investigated using a plate-like crystal with an area of approximately 18 mm^2 cut perpendicular to the $[0\,\bar{2}\,1]$-direction. The measurement was carried out on a D5000 diffractometer using CuK_α radiation. Low temperatures were reached via a helium-flow cryostat. The sample was placed in 50 mbar He-atmosphere.

For the x-ray diffraction experiment aiming at crystal-structure refinements, a much smaller crystal was needed. The crystals are easily destroyed by mechanical stress, and therefore the crystal for x-ray diffraction could not be cut from a large crystal. Instead, a small amount of solution of $Cs_2[FeCl_5(H_2O)]$ was evaporated and the growth was stopped after several minutes, when the grown crystallites had the appropriate size. A crystallite of about 200 μm diameter was chosen for x-ray diffraction figure 1(d). X-ray diffraction was carried out on a Bruker AXS Kappa APEX II four-circle x-ray diffractometer with a wavelength of 0.7 Å (MoK_α radiation). Low-temperature measurements were performed with an Oxford Cryosystems N-HeliX, in which the sample is placed in a stream of cold nitrogen. At room temperature, 45 336 reflections compatible with the C-centered orthorhombic cell were collected, 3059 of which are unique. At 100 K the c axis is doubled and the measurement was carried out with respect to a primitive unit cell, so 80 519 reflections were collected, 10 245 of which are allowed and unique in the low-temperature symmetry. Furthermore, the temperature dependence of the $(\bar{6}\ 7\ \frac{5}{2})$ reflection was investigated between 100 K and 200 K.

3. Results and discussion

3.1. Structural phase transition

3.1.1. Study of the structural phase transition by means of diffraction experiments. Both our x-ray and neutron diffraction experiments show reflections $(h\ k\ l)$ with half-integer l (figure 2) emerging at (157.6 ± 0.1) K, which indicates the occurrence of a structural phase transition in $Cs_2[FeCl_5(H_2O)]$. A critical power law of the form $b + A \cdot (T_S - T)^{2\beta}$ is fitted to the neutron diffraction data, where b is the background, A a scaling factor, T_S the transition temperature and β the critical exponent. An interval of 10 K above the transition temperature is excluded from the fit, because the diffuse scattering in this region would impair the fit analysis. The phase transition is clearly visible at (157.6 ± 0.1) K and the critical exponent can be determined to $\beta = 0.220 \pm 0.002$. The fit yields a much smaller error on the transition temperature, however we can estimate the precision of the temperature measurement to amount to 0.1 K. This transition temperature corresponds reasonably well to the structural phase transition temperature reported in 1987 by Chadwick and Thomas [16] by means of Mößbauer spectroscopy. The critical exponent and the form of the temperature dependence clearly indicate non-mean-field behavior. The transition seems to be essentially of second order involving only weak displacements, but the small exponent associated with the steep increase suggests some order-disorder character or strong coupling to strains. Assuming a continuous transition, it should be described by the condensation of a single phonon mode and the low-temperature space group should be an isotropy subgroup of *Cmcm* [20].

The superstructure reflections with non-integer l turned out to follow the selection rule $h + k = 2n + 1$ (for integer n), which corresponds to the violation of the C centering. This is only compatible to modes with propagation vector $(1\,0\,0.5)$

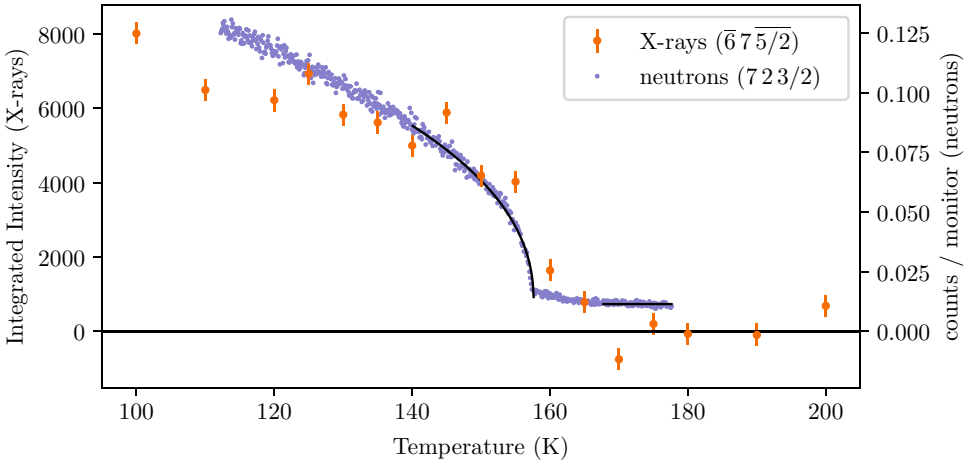

Figure 2. Temperature dependence of the $(\bar{6}\,7\,\overline{5/2})$-reflection by means of x-ray diffraction during heating and of the $(7\,2\,3/2)$-reflection by means of neutron diffraction during cooling. The line denotes a critical power law fit to the neutron intensities.

Table 1. Isotropy subgroups of the parent space group *Cmcm* describing the crystal structure of $Cs_2[FeCl_5(H_2O)]$ at high temperature [20]. Note that in all subgroups the low-temperature symmetry becomes either polar or monoclinic or both.

Mode	Monoclinic, centrosymmetric	Orthorhombic, polar	Monoclinic, polar
T_1	*C*2/*m*	*Imm*2	*Cm*
T_2	*C*2/*c*	*Ima*2	*Cc*

labeled T_1 and T_2 [20]. The possible low-temperature space groups arising from the condensation of one of these modes are summarized in table 1. For each mode symmetry, different low-temperature space groups are possible depending on the direction of the order parameter [20]. Note that the symmetry analysis unambiguously indicates that the low-temperature phase of $Cs_2[FeCl_5(H_2O)]$ is either monoclinic centrosymmetric, orthorhombic polar or monoclinic polar, see table 1. Therefore, it is essential to obtain a direct indication for either of these possibilities.

3.1.2. Pyroelectricity. In order to analyze the possibility of a polar low-temperature structure, we searched for the corresponding ferroelectric polarization. For the orthorhombic low-temperature space groups presented in table 1, the ferroelectric polarization must appear in the *b* direction of the high temperature *Cmcm* structure, see table 1. Therefore, we tested the pyrocurrent along this direction as depicted in figure 3. No pyroelectric current could be detected within the high sensitivity of our experiment. Typical multiferroic materials exhibit a ferroelectric polarization of several hundred $\mu C\ m^{-2}$ [21] and typical ferroelectrics even exceed such values by orders of magnitude. Such a ferroelectric polarization can be unambiguously ruled out for $Cs_2[FeCl_5(H_2O)]$. The high precision of our experiment gives a clear indication that the inversion symmetry is not broken during the structural phase transition at about (157.6 ± 0.1) K. The nearly constant current, which is smaller than the noise, is visible as a slope in the upper part of figure 3. It may be caused by the Seebeck effect due to temperature gradients or by ion exchange due to corrosion of contact surfaces. Furthermore, the operational amplifier exhibits a constant drift caused by the triboelectric effect. Nevertheless this measurement is very sensitive and excludes any ferroelectric polarization parallel $\boldsymbol{b}$ greater than $0.5\,\mu C\ m^{-2}$.

3.1.3. Microscopy using polarized light. Microscopical studies using polarized light are very sensitive to detect ferroelastic domains, which are expected to emerge at a transition from an orthorhombic to a monoclinic lattice. In the temperature interval 100–300 K, our polarization microscopy on $Cs_2[FeCl_5(H_2O)]$ shows neither an indication for the appearance of ferroelastic domains, nor a discontinuity in the optical image. The absence of an effect in polarization microscopy cannot fully exclude a monoclinic distortion. However, because polarization microscopy is very sensitive, any possible monoclinic deformation must be small. This assumption is further supported by a previous measurement of the magnetoelectric tensor at 5 K [4]: Only the components α_{12} and α_{21} significantly deviate from zero, whereas for the monoclinic symmetry in question also the components α_{23} and α_{32} are allowed to be non-zero. Again, this finding does not exclude a monoclinic distortion, but it is incompatible with a large deformation.

3.1.4. X-ray diffraction: $(0\,\bar{8}\,4)$ scan. For the monoclinic solutions given in table 1, the *a* axis of the *Cmcm* unit cell becomes the monoclinic axis. Therefore, any orthorhombic $(h\,k\,l)$ reflection will split into $(h\,k\,l)$ and $(h\,k\,\bar{l})$. This splitting is also observable in a single-crystal experiment, because ferroelastic domains will emerge at the orthorhombic to monoclinic transition. One of the reflections that are supposed to sizeably split is the $(0\,\bar{8}\,4)$ reflection. Figure 4(a) shows longitudinal scans across the $(0\,\bar{8}\,4)$ reflection as function of temperature. Above the phase transition, the $K_{\alpha_1} - K_{\alpha_2}$ splitting of the x-ray radiation is visible. Below the phase transition the peak width increases, so that the $K_{\alpha_1} - K_{\alpha_2}$ splitting becomes hidden in the single broader peak. Figures 4(b)–(d) show the results of pseudo Voigt fits to the data, which quantitatively confirm this observation. The position μ of the maximum corresponds to the $(0\,\bar{8}\,4)$ *d* value, and Γ is the full width at half maximum. For the fit two pseudo-Voigt functions were

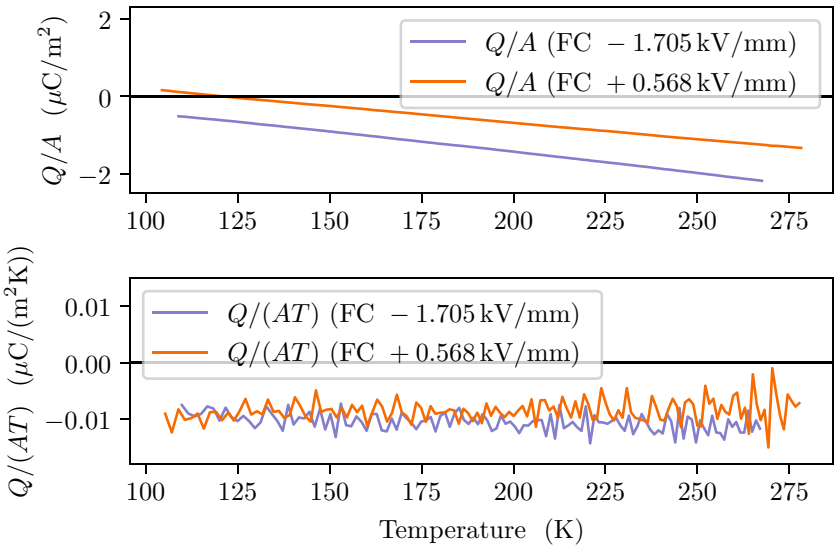

Figure 3. Pyroelectric measurement during heating parallel to the *b* direction (of the room temperature *Cmcm* structure). The sample was cooled in an electric field of 568 kV m^{-1} or 1705 kV m^{-1}, respectively, with different signs. The upper panel represents the integrated charge divided by the area and the lower part the pyrocurrent.

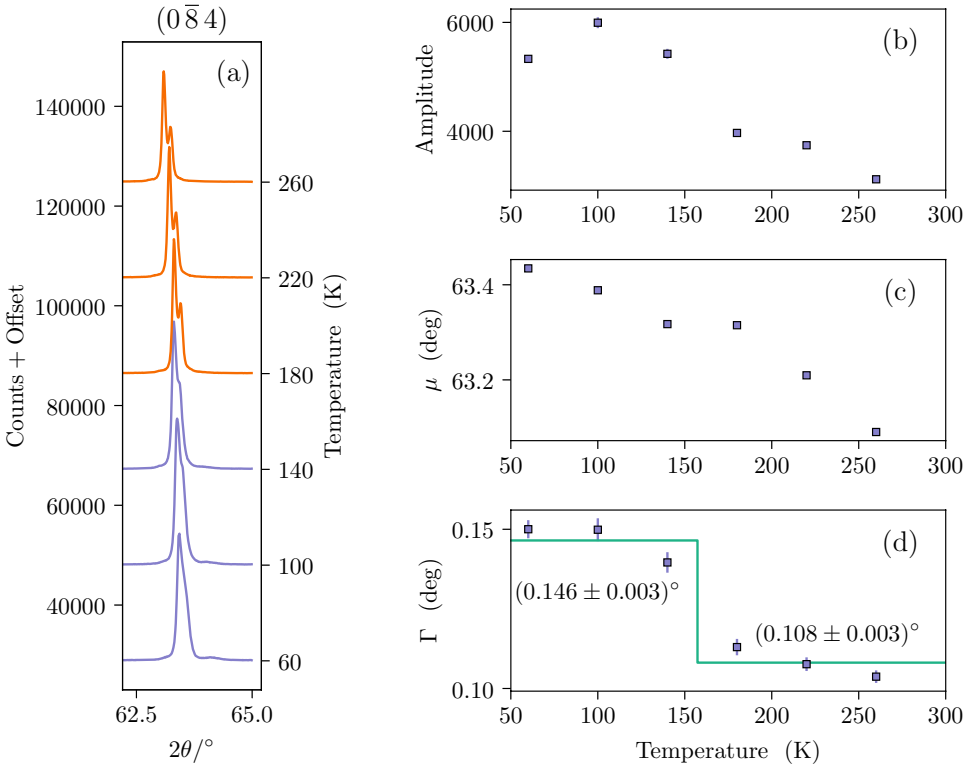

Figure 4. Temperature dependent x-ray diffraction of the $(0\,\bar{8}\,4)$ reflection. (a) Temperature resolved $(0\,2\bar{l}\,l)$ scan of the $(0\,\bar{8}\,4)$ reflection. (b)–(d) Parameters of the pseudo Voigt function fitted to the reflections. It can be seen that below the transition temperature of approx. 160 K, the peak width Γ increases with decreasing temperature. This is an indication for a very small monoclinic splitting.

added with a fixed intensity ratio of 100 : 51.5 and with the relative positions μ_1 and μ_2 fixed by the $K_{\alpha_1} - K_{\alpha_2}$ splitting [22]; all other parameters are kept equal.

In figures 4(b)–(d), it can be seen that with increasing temperature the amplitude decreases and the interplanar distance $d_{(084)}$ increases. The full width at half maximum Γ increases below the transition temperature between 140 K and 180 K. The behavior below the transition temperature indicates a very small monoclinic splitting. The monoclinic splitting is too small to become directly visible but results in a broadening of the reflection. The splitting is indeed very small: The angle α deviates from 90° by approximately 0.08° (in orthorhombic notation).

3.1.5. X-ray diffraction: structure determination. With the absence of ferroelectric polarization in the low-temperature

Table 2. Results of the structure refinements based on single crystal x-ray diffraction data of $Cs_2[FeCl_5(H_2O)]$ measured at room temperature and at 100 K.

Room temperature:

Space group		Cell parameters		*R*-values
Cmcm	*a*	= 7.4288(4) Å	*R*(obs)	= 2.57%
(orthorhombic)	*b*	= 17.3131(9) Å	w*R*(obs)	= 3.00%
	c	= 8.0696(4) Å	*R*(all)	= 5.99%
			w*R*(all)	= 3.38%

	x	y	z	Uiso	U11	U22	U33	U12	U13	U23
Cs1	0	0.470 605(11)	1/4	0.027 25(4)	0.031 72(8)	0.031 22(9)	0.018 82(7)	0	0	0
Cs2	0	0.754 766(12)	1/4	0.032 97(5)	0.029 77(9)	0.026 64(8)	0.042 51(11)	0	0	0
Fe1	0	0.121 785(19)	1/4	0.017 30(7)	0.019 27(13)	0.016 61(13)	0.016 02(12)	0	0	0
Cl1	0	0.253 61(4)	1/4	0.030 11(17)	0.0313(3)	0.0168(2)	0.0422(4)	0	0	0
Cl2	0.223 89(5)	0.111 41(2)	0.459 35(5)	0.030 79(9)	0.028 81(15)	0.034 63(17)	0.028 93(15)	0.005 90(12)	−0.012 09(12)	−0.001 95(13)
O1	0	0.995 80(12)	1/4	0.0314(6)	0.0576(15)	0.0169(8)	0.0197(8)	0	0	0

100 K:

Space group		Cell parameters		*R*-values
*I*2/*c*	*a*	= 17.1206(14) Å	*R*(obs)	= 3.17%
(monoclinic)	*b*	= 7.3619(6) Å	w*R*(obs)	= 3.94%
	c	= 16.086(4) Å	*R*(all)	= 4.75%
	β	= 90.000(14)°	w*R*(all)	= 4.19%

	x	y	z	Uiso	U11	U22	U33	U12	U13	U23
Cs1_1	−0.028 711(10)	0.521 78(3)	−0.125 101(16)	0.007 84(6)	0.009 96(6)	0.008 03(15)	0.005 52(5)	−0.000 32(4)	-0.000 45(6)	0.000 13(6)
Cs2_1	−0.256 319(11)	0.4892(4)	0.123 76(2)	0.009 43(18)	0.009 06(6)	0.0058(5)	0.013 43(6)	0.000 52(8)	0.000 11(6)	0.001 17(14)
Fe1_1	−0.121 707(18)	−0.0056(2)	−0.374 45(3)	0.005 45(6)	—	—	—	—	—	—
Cl1_1	−0.255 11(3)	0.0050(5)	−0.375 96(5)	0.011 12(12)	—	—	—	—	—	—
Cl2_1	−0.116 38(11)	−0.2316(2)	−0.274 73(10)	0.009 00(12)	0.010 55(18)	0.008 18(6)	0.0083(3)	0.000 35(9)	0.000 69(19)	0.002 20(17)
Cl2_2	−0.108 40(11)	0.2196(2)	−0.264 86(11)	0.009 00	0.010 55	0.008 27	0.0082	0.000 69	−0.000 35	−0.002 20
Cl2_3	−0.112 09(7)	0.241 89(14)	−0.472 35(7)	0.009 00	0.010 55	0.008 18	0.0083	0.000 35	0.000 69	0.002 20
Cl2_4	−0.109 08(7)	−0.210 25(14)	−0.485 93(7)	0.009 00	0.010 55	0.008 27	0.0082	0.000 69	−0.000 35	−0.002 20
O1_1	0.005 35(12)	−0.013(2)	−0.3746(2)	0.0071(15)	0.0055(6)	0.008(4)	0.0082(5)	−0.0002(8)	−0.0002(7)	0.0005(13)

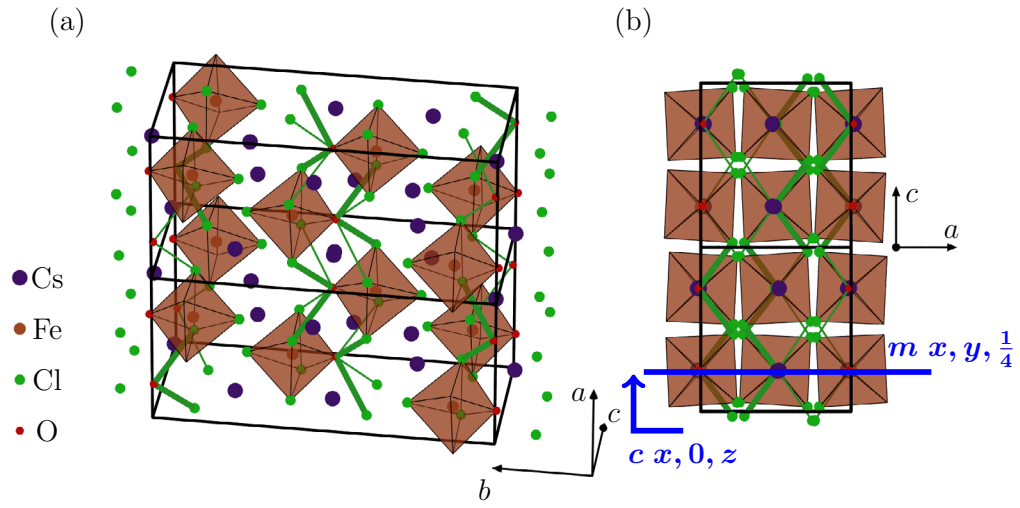

Figure 5. Crystal structure of $Cs_2[FeCl_5(H_2O)]$. (a) The phase transition induces an ordering of the O–H–Cl hydrogen bonds. Hydrogen bonds which are realized are displayed thicker than bonds which are not realized in the low temperature phase. (b) The phase transition breaks the mirror plane $m\ x, y, \frac{1}{4}$ and the glide plane $c\ x, 0, z$. The direction of view is the b axis of the *Cmcm* unit cell. The structure displayed is the *I*2/*c*-structure transformed to the unit cell of the *Cmcm*-structure. The octahedrons are rotated, so that the mirror plane and the glide plane are broken.

phase and with the indication for a monoclinic distortion there remain only two possible space groups *C*2/*m* (mode T_1) or *C*2/*c* (mode T_2), which were both tested by structural refinements with the comprehensive low-temperature data set. The R values amount to $R(\text{obs}) = 4.21\%$, $wR(\text{obs}) = 5.96\%$, $R(\text{all}) = 6.16\%$, and $wR(\text{all}) = 6.21\%$ for space group *C*2/*m* and to $R(\text{obs}) = 3.17\%$, $wR(\text{obs}) = 3.94\%$, $R(\text{all}) = 4.75\%$, and $wR(\text{all}) = 4.19\%$ for space group *C*2/*c*. Therefore, we can safely identify *C*2/*c* as the space group of the low-temperature phase.

It is important to note, that the structural refinements do not allow one to distinguish the different low-temperature space groups arising from the same symmetry but different order-parameter directions. For the two orthorhombic polar space groups arising from the same T_1 and T_2 modes, *Imm*2 and *Imma*, see table 1, we obtain the R values: $R(\text{obs}) = 4.30\%$, $wR(\text{obs}) = 5.89\%$, $R(\text{all}) = 6.49\%$, $wR(\text{all}) = 6.16\%$, and $R(\text{obs}) = 3.16\%$, $wR(\text{obs}) = 4.04\%$, $R(\text{all}) = 5.10\%$,$wR(\text{all}) = 4.34\%$,respectively,whicharealmost identical to those obtained for the corresponding non-polar solutions. Excluding the polar solutions through the absence of ferroelectric polarization is thus essential.

In order to facilitate the discussion we use the non-standard setting *I*2/*c* instead of *C*2/*c* in the following. We label the axes of the orthorhombic cell with symmetry *Cmcm* by $\boldsymbol{a}, \boldsymbol{b}, \boldsymbol{c}$, the axes of the monoclinic cell in the setting with symmetry *I*2/*c* by $\boldsymbol{a}^{\mathrm{M}}, \boldsymbol{b}^{\mathrm{M}}, \boldsymbol{c}^{\mathrm{M}}$ and the axes of the monoclinic cell in the standard setting *C*2/*c* by $\boldsymbol{a}^{\mathrm{S}}, \boldsymbol{b}^{\mathrm{S}}, \boldsymbol{c}^{\mathrm{S}}$. The axes of the setting *I*2/*c* are obtained from those of the setting *C*2/*c* via a shift of the origin to $(-1/4, -1/4, -1/2)^{\mathrm{T}}$ followed by a basis transformation $\boldsymbol{a}^{\mathrm{M}} = \boldsymbol{c}^{\mathrm{S}}$, $\boldsymbol{b}^{\mathrm{M}} = \boldsymbol{b}^{\mathrm{S}}$, $\boldsymbol{c}^{\mathrm{M}} = -\boldsymbol{a}^{\mathrm{S}} - \boldsymbol{c}^{\mathrm{S}}$. Starting from the high-temperature space group *Cmcm*, we yield the setting of *I*2/*c* by a simple basis transformation $\boldsymbol{a}^{\mathrm{M}} = \boldsymbol{b}$, $\boldsymbol{b}^{\mathrm{M}} = \boldsymbol{a}$, $\boldsymbol{c}^{\mathrm{M}} = -2\boldsymbol{c}$. In all figures we show the axes $\boldsymbol{a}, \boldsymbol{b}, \boldsymbol{c}$ according to the orthorhombic cell with space group *Cmcm*, so that in figures showing the monoclinic cell, the c axis extends only over half a unit cell.

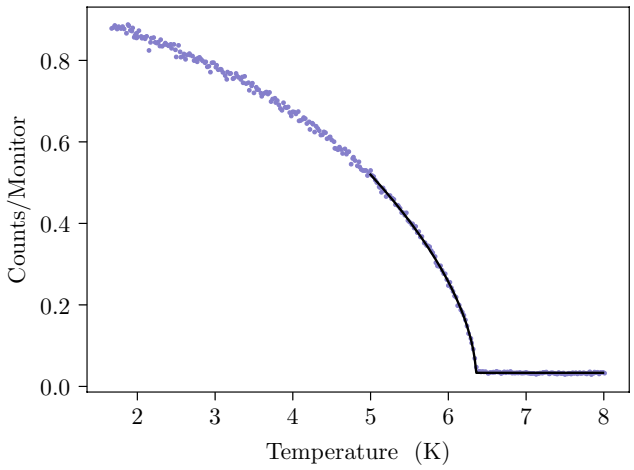

Figure 6. The (0 0 1)-reflection is not allowed in *Cmcm*-symmetry but appears at the magnetic phase transition at about (6.35 ± 0.05) K. The data were collected at the thermal neutron diffractometer 6T2. An exponential law was fitted similar to that in figure 2, resulting in an exponent of $\beta = 0.2890(2)$. The fit returns a much smaller error on the transition temperature, however we can assume a precision on the temperature of 0.05 K.

The atomic displacement parameters (ADPs) of Fe1_1 and Cl1_1 were refined isotropically, all other atomic displacement parameters anisotropically. The ADPs of the atoms Cl2_1, Cl2_2, Cl2_3 and Cl2_4, that occupy equivalent positions in the high temperature phase, are constricted in the following way: The ADPs of atom Cl2_1 equal the ADPs of atom Cl2_3 and the ADPs of atom Cl2_2 equal the ADPs of atom Cl2_4. Furthermore, the ADPs of atom Cl2_2 are the ADPs of atom Cl2_1 rotated by 90° around the a axis. The results of the structural refinements, both at room temperature and at 100 K, are shown in table 2.

When inspecting the room-temperature structural parameters in table 2 the large atomic displacement parameters (ADP) are remarkable. The isotropic averaged mean square displacements for all atoms are in the order of 0.02 to 0.03 $\mathring{A}^2$, which translates to root-mean-square displacements of the order of 0.1 Å. Such large values are well beyond the displacements caused by thermal activation of phonons but point to severe disorder in the room-temperature structure. The recent structure determination of the deuterated compound [15] reports very similar values, and the largest ADP, U_{11} of O, of about 0.06 $\mathring{A}^2$ perfectly agrees for the D and H compounds. The direction of the largest ADP of the O corresponds to the displacement of this ion in the low-temperature structure. The low-temperature distortion is therefore also present at room temperature as a local distortion. Clearly the disorder in the hydrogen bonding and in the position of the water molecules induces severe intrinsic disorder in the entire crystal structure of $Cs_2[FeCl_5(H_2O)]$ touching also the heavier atoms.

The crystal structure at 100 K was refined including a twinning law according to the twin matrix shown in equation (2):

$$\begin{pmatrix} h^{\mathrm{M}} \\ k^{\mathrm{M}} \\ l^{\mathrm{M}} \end{pmatrix}_{\mathrm{twin2}} = \begin{pmatrix} 1 & 0 & 0 \\ 0 & -1 & 0 \\ 0 & 0 & -1 \end{pmatrix} \begin{pmatrix} h^{\mathrm{M}} \\ k^{\mathrm{M}} \\ l^{\mathrm{M}} \end{pmatrix}_{\mathrm{twin1}} . \qquad (2)$$

The refinement yields a fraction of 0.22 for twin 2. The twinning corresponds to the emergence of ferroelastic domains at the orthorhombic to monoclinic phase transition. The fact that even the small x-ray crystal exhibits different domains strongly suggests that several thousands times larger crystals severely suffer from twinning, which needs to be taken into account in the interpretation of all former and future measurements.

The low-temperature structure is shown in figure 5(a). The octahedrons are rotated around $\boldsymbol{b}^{\mathbf{M}} = \boldsymbol{a}$ in a way that only one of the two Cl atoms of a neighboring octahedron approaches the O ion. This shorter distance results from the ordering of the O–H–Cl hydrogen bonds. While at room-temperature the distance between the O and each of the four Cl ions amounts 3.4205(14) Å, the distances considerably split at 100 K into two short and two long bonds. The short distances amount to 3.328(8) Å and 3.300(8) Å and the long distances to 3.460(7) Å and 3.499(8) Å, respectively. This splitting is remarkably strong and the mean distance considerably shrinks. Figure 5(b) illustrates the breaking of symmetries. The axes are the axes of the *Cmcm* cell doubled in *c* direction, however the structure corresponds to the low-temperature phase. The mirror planes and the glide plane shown in figure 5(b) are broken because of the $[FeCl_5(H_2O)]$ octahedron rotation. The angle of rotation can be determined by measuring the rotation of the octahedron edges which are parallel to the crystallographic axes in the high-temperature phase. Taking the mean of these four values, one yields an alternating rotation by 3.4(4)°. The sequence of the signs of the octahedron rotations are enforced by the water molecules. Two octahedra separated by one orthorhombic *c* spacing rotate in opposite sense, because the resulting hydrogen bonds better suite to the water molecule.

3.2. Magnetic phase transition

Figure 6 shows the temperature dependence for the intensity of the (0 0 1)-reflection. This reflection is forbidden in the orthorhombic *Cmcm* phase, and also in the monoclinic phase with symmetry *I*2/*c* it is weak. This reflection essentially appears at the magnetic phase transition at about 6.4 K. The critical exponent agrees reasonably well with the expectation for a three-dimensional Heisenberg system.

Considering the pure magnetic structure of $Cs_2[FeCl_5(H_2O)]$ in space group *Cmcm* and ignoring the structural distortion, the observation of the strong (0 0 1)-reflection indicates a $\boldsymbol{k} = \mathbf{0}$ structure with alignment of the moment perpendicular to $\boldsymbol{c}$. This is in accordance with the fact that the susceptibility drops below T_{N} for a magnetic field parallel to the *a* axis [4]. The symmetry analysis for $\boldsymbol{k} = \mathbf{0}$ in *Cmcm* is quite simple [23]: There are six representations each corresponding to a single magnetic component in one of the orthorhombic directions that is either ferromagnetic or antiferromagnetic for the two Fe sites related through the inversion symmetry. The two antiferromagnetic configurations with moments parallel *a* and *b* (representations Γ_2 and Γ_4) were tested. The magnetic structure refinement was carried out with the difference of the reflection intensities measured at 10 K (paramagnetic phase) and at 1.6 K (antiferromagnetic phase). The reflections used in the magnetic refinement were restricted to $2\theta < 30°$ because the intensity of magnetic reflections strongly decreases for high angles following the form factor squared. 116 reflections were used for the refinement. In order to determine the absolute value of the magnetic moment, a nuclear refinement was carried out with the data measured at 10 K, yielding *R*-Values of $R(F^2) = 13.1\%$ and $wR(F^2) = 16.1\%$. The magnetic refinement uses the scaling factor determined by the nuclear refinement. Refinements according to Γ_2 and Γ_4 yield $\chi^2 = 37$ and $\chi^2 = 1.7$, respectively, with a single magnetic parameter. The *R*-values amount to $R(F^2) = 62.9\%$ and $wR(F^2) = 68.6\%$ for Γ_2, and to $R(F^2) = 28.8\%$ and $wR(F^2) = 14.9\%$ for Γ_4. It is obvious that the magnetic structure can be described best in the irreducible representation Γ_4 corresponding to moments of $4.10(3)\mu_B$ along $\boldsymbol{a}$. The magnetic structure corresponds to the magnetic point group mmm' and Shubnikov group $Cmcm'$.

The ordered moment is lower than the effective moment of 5.92 μ_{B} determined from susceptibility data [4] and also below the expected value of 5 μ_{B} expected for a Fe^{3+}-ion in high-spin configuration ($S = 5/2$)[4] Also in the deuterated compound a smaller moment was detected [15][5]. A part of the missing moment can be explained by fluctuations but the larger fraction might arise from moments transferred to ligands that were not included in the refinements.

Taking the structural distortion into account, the representation analysis must be carried out in space group *I*2/*c* (standard setting *C*2/*c*). In this case, the irreducible representation Γ_4 permits the antiferromagnetic arrangement of moments along $b_{\mathrm{monoclinic}} = a_{\mathrm{orthorhombic}}$ shown in figure 7. In addition the lower symmetry allows for an admixture of a canting of the

[4] Note that the ordered moment compares to *S* and not to $\sqrt{S(S+1)}$.
[5] Fabelo *et al* discuss the magnetic structure in another setting, in which the moment points along *b*.

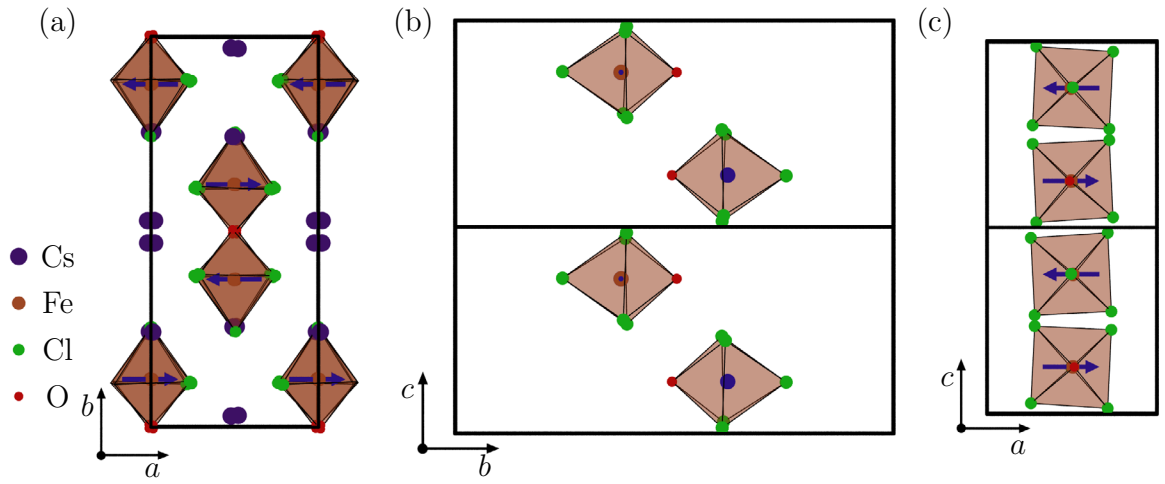

Figure 7. (a) Magnetic structure of $Cs_2[FeCl_5(H_2O)]$, view along c. The axes are the axes of the *Cmcm* high-temperature structure. The magnetic structure corresponds to that predicted by Ackermann *et al* [4] with moments aligned along $\boldsymbol{a}$ and Shubnikov group $Cmcm'$. The magnetic moments are canted away from the a axis, which is not displayed in this figure due to large uncertainties. (b) Four octahedrons of a zig-zag chain, coupled by O–H–Cl bonds, view along a. (c) The same octahedrons, view along b. It can be seen, that their magnetic moments order antiferromagnetically, while the tilts of the octahedrons are arranged in an 'up–up–down–down' pattern.

magnetic moments in b and c direction. However, our data do not allow a reliable refinement of the canted moments with satisfying error bars due to the twinning of monoclinic domains. The structural distortion seems to be too weak to posses a significant impact on the magnetic coupling, which also corresponds to the absence of significant α_{23} and α_{32} coefficients [4] on the magnetoelectric tensor. The proper magnetic space group including the structural transition is $I2'/c$. From the magnetic symmetry elements in the *Cmcm* structure, $C\frac{2'}{m}\frac{2'}{c}\frac{2_1}{m'}$, only the $2'$ axis along a is not broken at the phase transition and the mirror plane perpendicular to a is reduced to a glide-mirror plane with the doubled c parameter. The inversion symmetry in $I2/c$ connecting two Fe sites is coupled to time inversion in the antiferromagnetic chain. Therefore, the linear magnetoelectric effect is possible.

3.3. Comparision to existing structure analyses

Our results are compatible to the very recent publication of Fabelo *et al* [15]. There, the deuterated compound $Cs_2[FeCl_5(D_2O)]$ was investigated while we study the hydrogen compound, for which magnetoelectric data exist. The lattice parameters at room temperature deviate by several standard deviations from our data, which can be attributed to the deuterization. The room-temperature atomic positions and ADP's are in excellent agreement with our data. In particular the anomalously large anisotropic ADP's well agree for the two compounds studied with different techniques. Fabelo *et al* [15] report about 175 K for the transition temperature in the deuterated compound, significantly above the value of (157.6 ± 0.1) K for $Cs_2[FeCl_5(H_2O)]$. The low temperature crystal structure cannot be compared in such a high precision, because in [15] the crystal structure was determined at 20 K (in contrast to 100 K in the present study). However, most of the atomic positions deviate in the same direction with respect to the room temperature crystal structure yielding a qualitatively similar picture of the distortion. The rotation angle of the octahedron around the b direction can be obtained by averaging over the four edges. It amounts to 3.73(3)° in the deuterated compound at 20 K, while we find 3.4(4)° in the H material at 100 K. In the absence of any studies of ferroelectric polarization for the deuterated compound it is unclear whether a polar distortion can be excluded for this compound as well. It is noteworthy that the small y coordinates of the Fe atom and of the O atom at low temperature can be inverted without an increase of the R values in the refinement. This is remarkable, because the resulting structures are different. The magnetic structure and the magnetic transition temperature are in agreement with the work of Fabelo *et al*. The ordered moment of 4.10(3) μ_B for the H compound is only slightly lower than the value given in [15] (4.39 μ_B) for the deuterated material.

4. Conclusion

The present investigations reveal that the structural phase transition occurring in $[FeCl_5(H_2O)]$ at approximately (157.6 ± 0.1) K doubles the c axis and lowers the symmetry from *Cmcm* to $I2/c$ (with a change of the origin and the basis vectors). During this transition, the $[FeCl_5(H_2O)]$ octahedrons rotate by 3.4(4)° around the b axis, accompanied by the ordering of H_2O molecules and of the related O–H–Cl hydrogen bonds. A significant ferroelectric polarization can be excluded at this transition. The structural transition temperature is compatible with the transition temperature of 151.5 ± 0.5 K determined by Mößbauer spectroscopy [16]. Below 6.4 K, magnetic moments order antiferromagnetically along $\boldsymbol{a}$ described in Shubnikov group $Cmcm'$ ($I2'/c$ when considering the structural distortion) in perfect agreement with measurements of the magnetoelectric tensor. The structural distortions—although being sizeable—possess little impact on the magnetic and magnetoelectric properties.

Acknowledgment

This work was supported by the Deutsche Forschungsgemeinschaft through CRC 1238 Projects No. A02 and No. B04.

ORCID iDs

Tobias Fröhlich https://orcid.org/0000-0002-3547-1991
Jonas Stein https://orcid.org/0000-0001-7136-5419

References

[1] Figgis B N, Raston C L, Sharma R P and White A H 1978 *Aust. J. Chem.* **31** 2717–20
[2] Lacková D, Ondrejkovičová I and Koman M 2013 *Acta Chim. Slovaca* **6** 129–32
[3] Ackermann M, Brüning D, Lorenz T, Becker P and Bohatý L 2013 *New J. Phys.* **15** 123001
[4] Ackermann M, Lorenz T, Becker P and Bohatý L 2014 *J. Phys.: Condens. Matter* **26** 506002
[5] Luzón J, Campo J, Palacio F, McIntyre G J and Millán A 2008 *Phys. Rev.* B **78** 054414
[6] Carlin R L and O'Connor C J 1981 *Chem. Phys. Lett.* **78** 528–30
[7] McElearney J N and Merchant S 1978 *Inorg. Chem.* **17** 1207
[8] O'Connor C J, Deaver B S Jr and Sinn E 1979 *J. Chem. Phys.* **70** 5161–7
[9] Puértolas J A, Navarro R, Palacio F, Bartolomé J, González D and Carlin R L 1958 *Phys. Rev.* B **31** 516–26
[10] Greedan J E, Hewitt D C, Faggiani R and Brown I D 1980 *Acta Cryst.* B **36** 1927–9
[11] Sergienko I and Dagotto E 2006 *Phys. Rev.* B **73** 094434
[12] Gabás M, Palacio F, Rodríguez-Carvajal J and Visser D 1995 *J. Phys.: Condens. Matter* **7** 4725–38
[13] Campo J, Luzón J, Palacio F, McIntyre G J, Millán A and Wildes A R 2008 *Phys. Rev.* B **78** 054415
[14] Schultz A J and Carlin R L 1995 *Acta Cryst.* B **51** 43–7
[15] Fabelo O, Rodríguez-Velamazán J A, Canadillas-Delgado L, Mazzuca L, Campo J, Millán A, Chapon L C and Rodríguez-Carvajal J 2017 *Phys. Rev.* B **96** 104428
[16] Chadwick J and Thomas M F 1987 *J. Phys. C: Solid State Phys.* **20** 3979–83
[17] Balents L 2010 *Nature* **464** 199–208
[18] Puértolas J A, Navarro R, Palacio F, Bartolomé J and González D 1982 *Phys. Rev.* B **26** 395–403
[19] Johnson J A, Johnson C E and Thomas M F 1987 *J. Phys. C: Solid State Phys.* **20** 91–109
[20] Stokes H T and Hatch D M 1988 *Isotropy Subgroups of the 230 Crystallographic Space Groups* (Singapore: World Scientific)
[21] Stein J, Baum M, Holbein S, Cronert T, Hutanu V, Komarek A C and Braden M 2015 *J. Phys.: Condens. Matter* **27** 446001
[22] Bearden J A 1967 *Rev. Mod. Phys.* **39** 78–124
[23] Rodriguez-Carvajal J 1993 *Physica* B